Measurements of the AMSU-B Antenna Pattern

Timothy J. Hewison and Roger Saunders

Abstract—**Measurements of the antenna patterns for the high frequency component of the Advanced Microwave Sounding Unit (AMSU-B), to fly on the NOAA–KLM polar orbiting satellites, are reported here. They were made on the Compact Antenna Test Range at Queen Mary and Westfield College, London, at three frequencies within the AMSU-B receiver's channels, centered at 89, 150, and 183.31 GHz. The main reflector of AMSU-B's antenna is an offset parabola with a 219-mm diameter aperture. This paper describes the measurements that were made and presents the results of an analysis of them for the three AMSU-B flight models. Measurements of beamwidths, main beam efficiencies, and sensitivity to cross-polarization are all reported. These data are then used to compute simulated antenna temperatures for the space and Earth views and recommendations for correcting the space view and Earth view data due to antenna effects are proposed. The implications for the operational radiometric calibration of AMSU-B are also discussed.**

I. Introduction

THE U.K. Meteorological Office (UKMO) has procured the high frequency component of the Advanced Microwave Sounding Unit (AMSU-B) to fly on the new generation of NOAA operational polar orbiting satellites, NOAA's K, L, and M. The launch of the first satellite in this series, NOAA-K, is currently scheduled for launch in late 1996. One engineering model (EM) and three flight models (referred to as PFM, FM2, and FM3) were supplied by Matra Marconi Space, MMS, (formerly British Aerospace Space Systems Ltd.) and delivered to the UKMO during 1992–1994.

AMSU-B consists of a passive five-channel total power microwave radiometer with main scanning antenna inclined at 45° to direct the Earth's emitted radiation into the receiver. It has five separate channels with frequencies centered on 89, 150, 183.31±1, 183.31±3, and 183.31±7 GHz, hereafter referred to as channels 16, 17, 18, 19, and 20, respectively. The first two of these channels are at frequencies which have relatively low atmospheric absorption affected only by the contributions from water vapor and oxygen line wings. The three high frequency channels are centered on the 183.31 GHz water vapor absorption line to facilitate retrieval of atmospheric water vapor profiles. The AMSU-B channels will also allow the identification of precipitation, snow, and ice, and when used in conjunction with the lower frequency component, AMSU-A will allow global soundings of atmospheric temperature, humidity, and cloud liquid water path. More detailed information on the AMSU-B radiometer and its radiometric performance is reported elsewhere [1].

Manuscript received January 24, 1995; revised September 26, 1995.

The authors are with the U.K. Meteorological Office, Remote Sensing Instrumentation DRA, Farnborough, Hants GU14 6TD U.K. (e-mail: tjhewison@meto.govt.uk).

Publisher Item Identifier S 0196-2892(96)01014-5.

It is important to have a good knowledge of the antenna characteristics of all the AMSU radiometers in order to assess the effect on radiometric calibration, correct Earth radiances for cold space seen by the side lobes, and optimize remapping of the data to other instrument fields of view. This information has been difficult or impossible to obtain for the current series of microwave sounders. The purpose of this paper is to document the antenna measurements for all three AMSU-B flight models to allow future users of the data to take into account antenna effects when deriving products from AMSU-B data.

MMS have carried out a comprehensive measurement program of the far field AMSU-B antenna beam patterns on a compact antenna test range to demonstrate the flight models meet the specifications laid down by the UKMO. The results of the analysis carried out by the UKMO on these measurements for the three flight models are reported here together with calculations of the effect of the antenna pattern on the radiometric calibration. Antenna measurements of the AMSU-A radiometers with channels in the range 23–90 GHz have also been made and are reported in [2].

II. Description of the AMSU-B Antenna System

The AMSU-B antenna system consists of an offset paraboloidal beryllium main reflector, housed in a cylindrical shroud with a 219-mm diameter aperture. The surface roughness was specified to be <0.4 μm and the overall departure from a paraboloid to be <10 μm. The main reflector directs radiation on to a fixed secondary hyperbolic mirror and then into the quasi-optical system, where it is divided by two dichroic filter plates via a series of beam folding mirrors into three separate corrugated feed-horns. In this way, all channels are multiplexed on to a common beam axis and all should have the same far-field beamwidth, although they have very different centre frequencies (89, 150, and 183.31 GHz). The design of the antenna system of AMSU-B is described in full by Martin and Hall in [3].

The main reflector makes one complete rotation every $\frac{8}{3}$ s to direct radiation in a plane perpendicular to the satellite track on to the secondary mirror. During one rotation of the reflector 90 Earth views within ±48.95° of nadir are sampled, each separated by 1.10°, which are referred to as pixels 1 to 90. An internal calibration target at 180° from nadir and space in one of four possible viewing directions between 65 and 81° from nadir is also viewed, which are used as radiometric calibration points. The rotation rate is nonuniform to maximize the time for viewing the Earth and calibration views. The polarization vector rotates with antenna scan angle from "vertical" at nadir (i.e., when the electric field vector is perpendicular to the

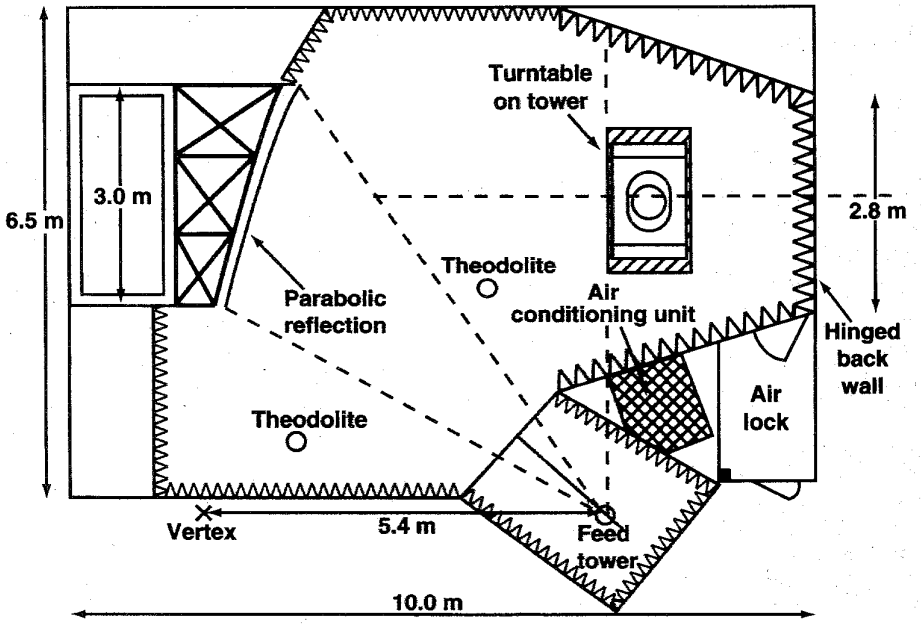

Fig. 1. Plan of QMW compact antenna test range.

direction of satellite motion) to "horizontal" at ±90° from nadir.

In order to meet the accuracy requirement for the main products (i.e., temperature and humidity profiles), the antenna of each AMSU-B flight model must meet a series of specifications defined by the UKMO, based on simple criteria listed below.

i) The full-width half-power beamwidth of all AMSU-B channels in any plane should be within ±10% of 1.10°. This translates into an area 16 km in diameter at the subsatellite point for the NOAA satellite orbital altitude of ~850 km.

ii) The main beam efficiency must be greater than 95%. This is defined as the fraction of the total radiant energy that is received from the main beam, which is a cone of half-angle equal to 1.25 times the measured averaged half-power beamwidth (i.e., half angle 1.375° for an ideal beamwidth of 1.1°). In addition more than 99% of the received power must originate from a cone of half-angle of 4°. This is defined as the wide beam efficiency.

iii) The cross-polarization content is defined as the fraction of total power within the main beam that is detected in the orthogonal polarization. This must be less than 2% for the window channels (16 and 17) and 10% for the broadest of the channels centered on the water vapor line (i.e., channel 20). It is unspecified for the other two channels, as these are not expected to be sensitive to surface polarization effects.

III. The Compact Antenna Test Range

The use of a far-field range is not feasible for this instrument because of the variable absorption due to atmospheric water vapor, which would affect any outdoor test range. Given the size of the antenna, then at 89 GHz, the far field is beyond 30 m. Hence, each model of AMSU-B was tested on a specially modified Compact Antenna Test Range (CATR) at Queen Mary and Westfield College, London, to verify that they comply with the above specifications. In this facility, a test source, mounted in a feed tower, irradiates a 3-m aperture offset paraboloidal reflector. This forms a plane wave over the 1-m^3 "quiet zone," where the antenna under test is positioned. In the test area, the maximum peak-to-peak field ripple is typically 0.44 dB at 90 GHz and 1.0 dB at 180 GHz [4]. The CATR configuration is shown in Fig. 1 and described in more detail by Parini and Olver [4].

The test source can be rotated to locate the plane of polarization of the antenna under test and to allow its response to be measured in two orthogonal polarizations. Channel 16 of AMSU-B was tested in its lower sideband, using a 87.9-GHz Gunn oscillator. A 74.4-GHz Gunn oscillator with a frequency doubler was used to test channel 17 in its lower sideband at 148.8 GHz. Channel 19 in its upper sideband at 186.3 GHz was selected to test the high frequency channels using a doubled 93.15-GHz Gunn oscillator. A full description of the Tx/Rx systems can be found in [5]. The CATR parabolic reflector consists of 18 panels, each with a measured rms surface accuracy of 15 μm. However, there are 2- to 3-mm gaps between these panels, which produce a diffraction pattern in the measured antenna response as described in [6] (see Section IV for treatment of these "range effects").

The instrument was mounted on an azimuth over elevation turntable in the quiet zone. The antenna was parked in the required view and the receiver output from the channel under test was recorded while the turntable mapped out the antenna pattern by sampling it at fixed elevation intervals in consecutive lines of azimuth scans.

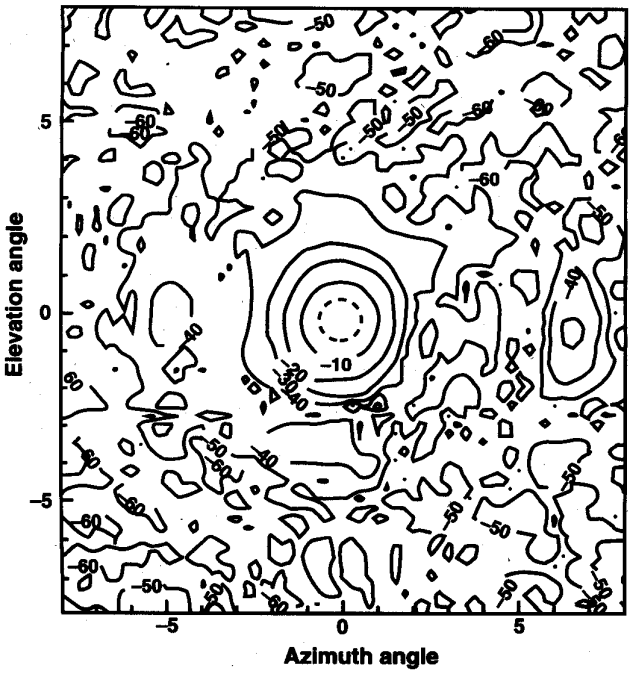

Fig. 2. Measured coarse antenna response for PFM channel 17 at nadir.

IV. Antenna Measurements

Measurements were made on the AMSU-B engineering model and all three flight models at QMW during 1992 and 1993. Coarse patterns were always mapped out in both polarizations (co- and cross-polar) with the antenna parked in nadir position (pixel 45). These covered ±35° in azimuth and elevation with a resolution of 0.25°, and are used to estimate the total power received by the antenna for all antenna positions and to check no significant side-lobes were present outside the main beam. Single azimuth cuts corresponding to along the scan direction were extended to ±90° to check no sidelobes were present beyond the sampled antenna pattern. For PFM these cuts were done for pixels 1, 45, 90, and space view. It was not possible to go beyond ±35° in the elevation plane (i.e., along the satellite track) because of constraints with the turntable. All the measurements were made with a dynamic range of >65 dB to ensure the main beam efficiency could be inferred to the required accuracy.

Fig. 2 shows a two-dimensional plot of the copolar coarse pattern for PFM channel 17 at nadir for the PFM. Note the apparent sidelobes at ~±6° in azimuth, with magnitudes of −35 dB. Fig. 3(a) shows an azimuth cut through the beam axis of the copolar pattern in Fig. 2 which shows the side lobes much more clearly. By repeating this measurement with the instrument in a slightly different position within the quiet zone, the side lobes were observed to shift relative to the beam centre. This is evidence that these are due to the diffraction pattern produced by the gaps in the CATR reflector rather than features of the antenna pattern itself. These first order range effects are removed from the copolar coarse antenna patterns by the following procedure. The positions of the first two maxima beyond the main beam in each plane are found.

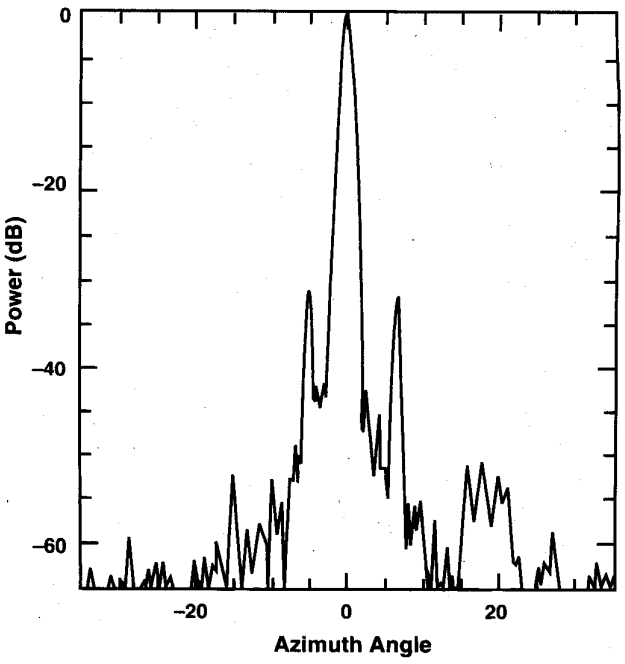

(a)

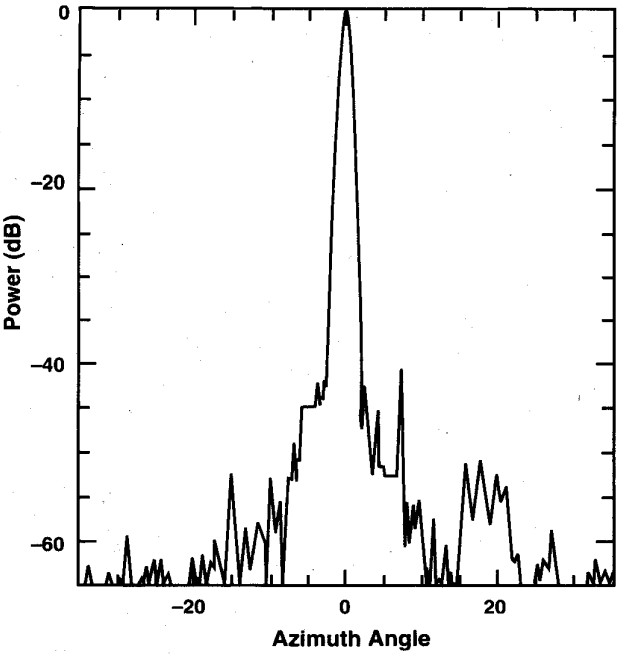

(b)

Fig. 3. Azimuth cuts through plot in Fig. 2 before and after correction of range effects.

Linear interpolation is applied between points on either side of strips 2° wide, 12° long, and centered on these maxima to remove them from the patterns. The result of this process on the same data-set is shown in Fig. 3(b).

Finer resolution patterns (0.05° resolution) were also measured, covering only a ±2° square centered on the beam axis for pixels 1, 45, and 90. From these, the beamwidths are

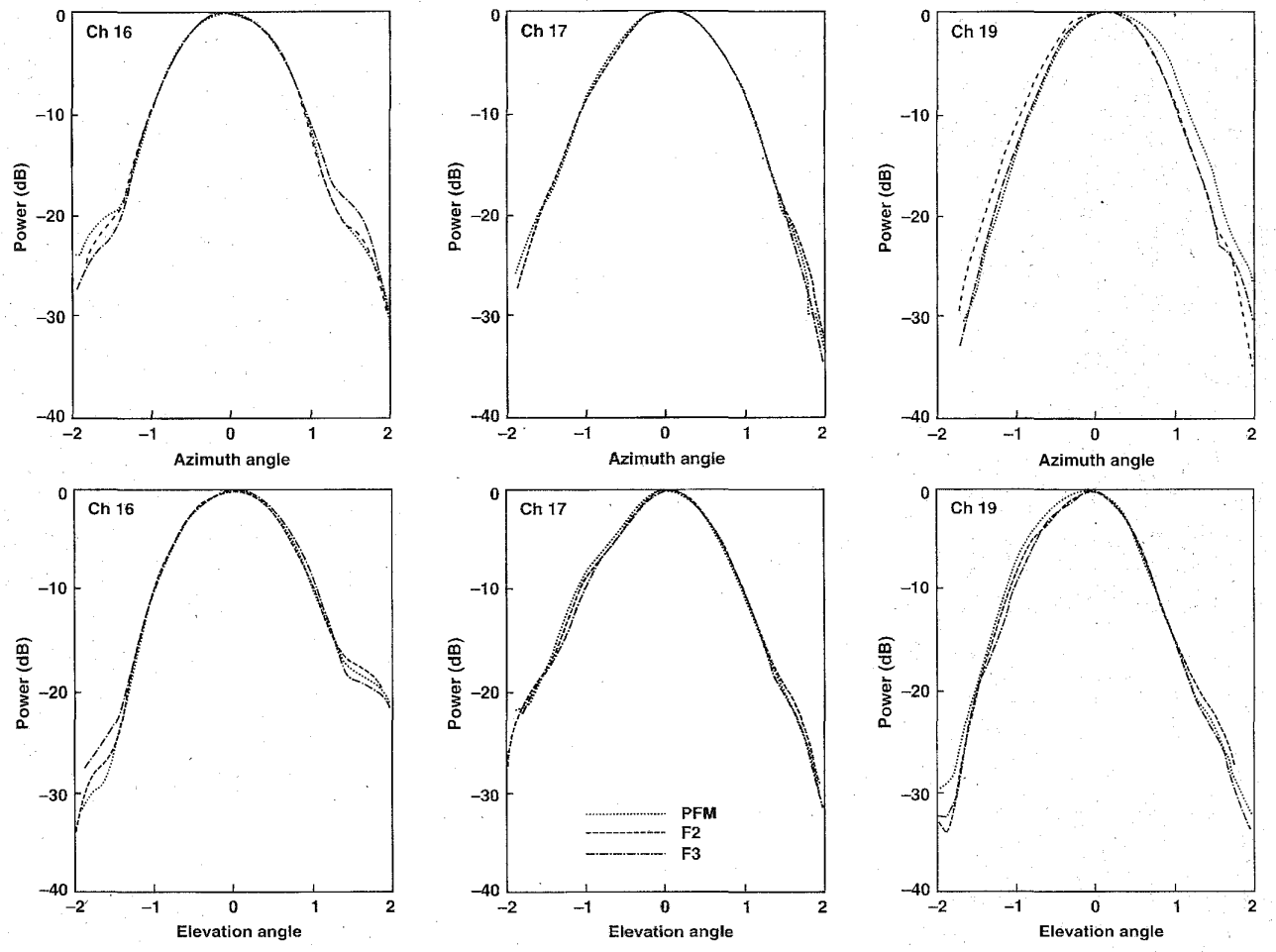

Fig. 4. Measured fine resolution cuts through the main beam for all three flight models with the antenna pointing at nadir.

calculated in two planes through the beam axis. These data are also used to calculate the power within the main beam area and the cross polarization, where both polarization patterns were measured. Examples of both azimuth and elevation cuts through the fine patterns are shown in Fig. 4 for all three flight models. The variations between models is small but measurable. The higher sidelobes of channel 16 are clearly evident in this figure.

V. Data Analysis

Following the notation of Ulaby *et al.* [7], two orthogonally polarized radiation patterns are measured to determine the complete normalized radiation pattern $F_n(\theta, \phi)$ required

$$F_n(\theta, \phi) = F_n^{\text{co}}(\theta, \phi) + F_n^{\text{cross}}(\theta, \phi) \tag{1}$$

where F_n^{co} and F_n^{cross} are the measured co- and cross-polarized components of the pattern, respectively, normalized with respect to the copolar maximum, and θ and ϕ are the elevation and azimuth angles relative to the beam axis where they are both zero (note these are not the usual spherical coordinates). Elevation θ ranges from -90 to $+90°$ and azimuth ϕ from -180 to $+180°$. These radiation patterns are corrected to remove the range effects as described in Section IV.

A. Beamwidths

The half-power beamwidths, θ_{bw} and ϕ_{bw} in the elevation and azimuth planes through the beam axis, are defined as the angular width between two angles at which the magnitude of $F_n(\theta, \phi)$ is equal to half its peak value

$$F_n(\theta_{\text{bw}}/2, 0) = F_n(0, \phi_{\text{bw}}/2) = 0.5. \tag{2}$$

Linear interpolation of the fine antenna patterns is used to calculate the beamwidths listed in Table I.

B. Beam Efficiencies

The antenna pattern solid angle, Ω_p, is defined by [7] as

$$\Omega_p = \int\int_{4\pi} F_n(\theta, \phi) d\Omega. \tag{3}$$

In CATR coordinates, the elemental solid angle, $d\Omega = \cos(\theta) \cdot d\theta \cdot d\phi$.

In our analysis this is approximated by

$$\Omega_p \sim \int_{-35°}^{+35°} \int_{-35°}^{+35°} F_n(\theta, \phi) \cdot \cos(\theta) d\theta d\phi \tag{4}$$

TABLE I
MEASURED AMSU-B HALF-POWER BEAMWIDTHS IN DEGREES

Channel	Freq.[GHz]	Pixel	Plane	PFM	FM2	FM3	Spec.
16	87.9	1	Az	1.15	1.15	1.18	
			El	1.11	1.11	1.15	
16	87.9	45	Az	1.10	1.12	1.13	1.10
			El	1.14	1.13	1.17	±0.11
16	87.9	90	Az	1.13	1.13	1.17	
			El	1.12	1.12	1.16	
17	148.8	1	Az	1.10	0.99	0.99	
			El	1.02	1.01	1.02	
17	148.8	45	Az	1.17	1.16	1.12	1.10
			El	0.99	0.99	0.96	±0.11
17	148.8	90	Az	1.05	1.04	1.09	
			El	1.03	1.05	1.00	
19	186.3	1	Az	1.20	1.06	1.05	
			El	1.08	1.03	1.03	
19	186.3	45	Az	1.18	1.14	1.08	1.10
			El	1.07	0.96	0.97	±0.11
19	186.3	90	Az	1.02	0.99	1.06	
			El	1.05	1.08	1.00	

which can be calculated from the co- and cross-polar coarse pattern data, substituting the central areas with fine patterns where available. The response beyond ±35° is assumed to be negligible and for the azimuth direction at least the cuts out to ±90° confirm that this assumption is reasonable.

The main beam solid angle, Ω_{MB}, is defined as

$$\Omega_{\mathrm{MB}} = \iint_{\mathrm{MB}} F_n(\theta,\phi)d\Omega \tag{5}$$

where MB is the main beam area defined as a cone of half-angle equal to 1.25 times the measured mean beamwidth.

This can be calculated from the fine pattern measurements and thus allows the calculation of the main beam efficiency, η_{MB}, defined as the ratio of the main beam to complete antenna pattern solid angles

$$\eta_{\mathrm{MB}} = \frac{\Omega_{\mathrm{MB}}}{\Omega_p}. \tag{6}$$

The wide beam efficiency, η_{WB}, is similarly defined as the ratio of the wide beam solid angle, Ω_{WB}, to the complete pattern solid angle. This must be calculated by combining the fine and coarse patterns. It is defined as

$$\Omega_{\mathrm{WB}} = \int_{-4^\circ}^{+4^\circ}\int_{-4^\circ}^{+4^\circ} F_n(\theta,\phi)d\Omega \tag{7}$$

where WB is the wide beam area, defined as a cone of half-angle equal to 4°. The wide beam efficiency is then defined as

$$\eta_{\mathrm{WB}} = \frac{\Omega_{\mathrm{WB}}}{\Omega_p}. \tag{8}$$

C. Cross Polarization

The cross-polarization content, η_{cross}, is defined as the ratio of the measured power in the main beam of the cross-polarization component to the total power in the main beam

$$\eta_{\mathrm{cross}} = \frac{\iint_{\mathrm{MB}} F_n^{\mathrm{cross}}(\theta,\phi)d\Omega}{\Omega_{\mathrm{MB}}}. \tag{9}$$

TABLE II
MEASURED AMSU-B MAIN BEAM AND WIDE BEAM EFFICIENCIES

Main Beam Efficiencies						
Channel	Freq.[GHz]	Pixel	PFM	FM2	FM3	Specification
16	87.9	45	94.4	94.4	94.9	>95.0
17	148.8	45	95.1	94.9	94.9	>95.0
19	186.3	45	96.9	96.2	96.5	>95.0
Wide Beam Efficiencies						
Channel	Freq.[GHz]	Pixel	PFM	FM2	FM3	Specification
16	87.9	45	98.36	98.43	98.33	>99.00
17	148.8	45	99.45	99.53	99.56	>99.00
19	186.3	45	99.64	99.15	99.15	>99.00

This is calculated from the fine resolution patterns measured in both polarizations where available.

VI. RESULTS

The measurements described in Section IV were analyzed independently both by MMS [5] and the UKMO and the two sets of results showed good agreement though with small differences due to the different analysis procedures. The results presented here are from the UKMO analysis. Table I summarizes the measured beamwidths for all three flight models (PFM, FM2, and FM3) and shows that channel 16 is consistently broader than the nominal 1.10°, especially at the scan extremes, though always within the specified limits and symmetric. The beamwidths of channels 17 and 19 at nadir in the elevation plane are just narrower than the original specification on the later flight models but the impact on the retrievals was calculated to be negligible. These beamwidths have an accuracy of $(^{+0.00}_{-0.01})^\circ$.

Table II lists the calculated main beam and wide beam efficiencies (η_{MB}, η_{WB}) for all AMSU-B flight models. Channel 16 consistently just fails to meet the original specifications, though these were the most technically difficult to achieve, due to the broader quasi-optic beam of this channel. However, from the extensive knowledge of performance acquired through these tests, operational corrections can be applied to achieve acceptable results (see Section VII) and so the specification was relaxed in this case. The engineering model beam efficiencies were measured in both pixels 1 and 45, and showed no significant difference in beam efficiency along the scan. The finite size of the antenna patterns and their limited dynamic range of 65 dB introduce an uncertainty of $(^{+0.4}_{-0.6})\%$ on the main beam efficiencies and $(^{+0.08}_{-0.13})\%$ on the wide beam efficiencies.

The cross-polarization contents, η_{cross}, listed in Table III, show that all views tested meet the specifications, except channel 17 in pixel 1. An impact analysis for this case showed this would produce a worst case uncertainty of 0.4 K in brightness temperature at the edge of the swath. Channel 16 of the engineering model was measured in both pixels 1 and 45 and showed low cross-polarization figures in both cases. These results have an accuracy of ±0.05%.

VII. ANTENNA TEMPERATURE PREDICTIONS

The implications of the measured performance of the antennas and the effect on the radiometric calibration are assessed in this section.

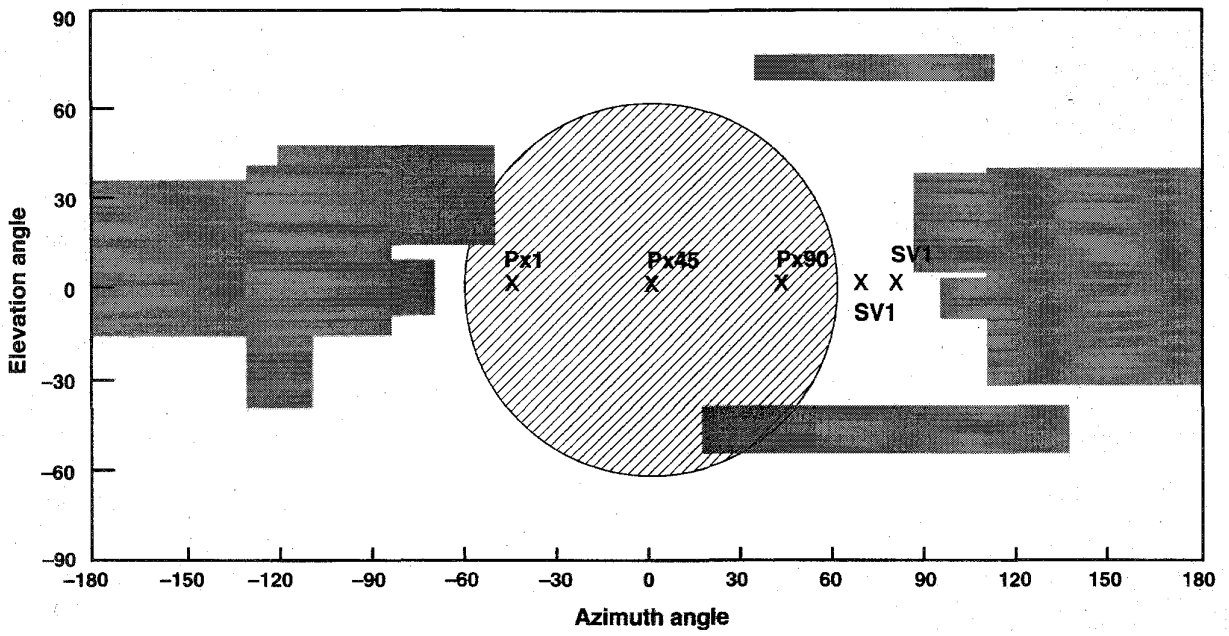

Fig. 5. Map of apparent temperature distribution for NOAA–KLM platform around AMSU-B scan.

TABLE III
MEASURED AMSU-B CROSS-POLARIZATION CONTENTS

Channel	Freq.[GHz]	Pixel	PFM	FM2	FM3	Specification
16	87.9	1	-	-	-	<2.0
		45	0.2	0.3	0.2	
		90	-	-	-	
17	148.8	1	2.4	2.3	2.3	<2.0
		45	0.5	0.8	0.6	
		90	1.0	1.1	1.3	
19	186.3	1	1.0	0.7	0.9	<10.0 for Ch.20
		45	0.5	0.3	0.2	
		90	-	1.7	1.6	

A. Theory

For distant objects (>30 m), the antenna radiometric temperature, T_A, can be calculated by convolving the antenna pattern, $F_n(\theta,\phi)$, with an assumed far-field radiance distribution, $B(\nu, T_{\rm AP}(\theta,\phi))$ [7] where ν is the channel frequency and $T_{\rm AP}$ is the assumed temperature distribution of the far field. The resulting antenna temperature is expressed in terms of temperature, by application of the inverse Planck function

$$T_A = B^{-1}\left\{\frac{\int_{4\pi}\int_{4\pi} B(\nu, T_{\rm AP}(\theta,\phi))F_n(\theta,\phi)\cdot\cos(\theta)d\theta d\phi}{\Omega_p}\right\} \tag{10}$$

where $B(\nu,T)$ and $B^{-1}(\nu,T)$ are the Planck function and its inverse. The calculation is in terms of radiance rather than brightness temperature because the Rayleigh–Jeans approximation breaks down for low brightness temperatures at AMSU-B frequencies. Equation (10) can be used to predict the extent of the bias of the measured antenna temperature due to antenna sidelobes being exposed to contrasting scenes. Such systematic errors will affect all Earth and space views to varying degrees. T_A is estimated using the coarse resolution antenna patterns, $F_n(\theta,\phi)$, which are available only over a $\pm 35°$ square centered on the beam axis. A map of the apparent temperature distribution $T_{\rm AP}(\theta,\phi)$ for the NOAA–KLM satellites is shown in Fig. 5. This is based on a crude projection of other instrumentation onboard the satellite and the silhouette of the Earth, against the cosmic microwave background of 2.73 K. The satellite instrumentation is assumed to have surfaces reflecting the Earth radiance but any secondary effects of reflected solar radiation are not included. It is important to note that the above assumes that all radiation sources are in the far field. The satellite instrumentation seen will be in the near field so the results of the calculations presented below are subject to some error due to this approximation and so the following calculations only give an approximate estimate of the effects of the side lobes. However, it is believed to be useful to estimate the magnitude of the effects of the side lobes even though the method of calculation is approximate.

It is possible to write this integration as a combination of the efficiency with which the antenna detects the Earth, η_E, the satellite platform, η_P, and space, η_S. These efficiencies vary according to which Earth or space view, v, is being considered

$$T_A = B^{-1}\{\eta_E(v)\cdot B(\overline{T_E}) + \eta_P(v)\cdot B(\overline{T_P}) + \eta_S(v)\cdot B(\overline{T_S})\} \tag{11}$$

where $\overline{T_E}$, $\overline{T_P}$, and $\overline{T_S}$ are the average apparent temperatures of the Earth, the satellite platform, and space, respectively. If η_E, η_P, and η_S are computed from (10) then T_A can be computed for various assumed values of $\overline{T_E}$ and $\overline{T_P}$.

B. Results

1) Effect on Space Views: To illustrate the effect of the response in the antenna sidelobes, Fig. 6 shows the predicted brightness temperatures for all four space views for channels

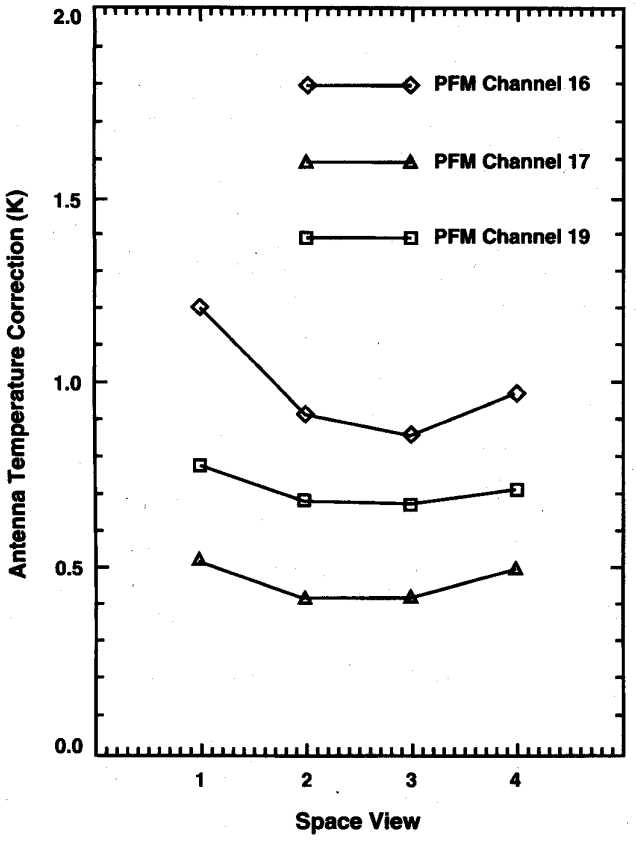

Fig. 6. Predicted antenna temperature corrections for the 4 space views for channel 16 ◇, channel 17 △, and channel 19 □ of the AMSU-B PFM. The correction should be added to the measured brightness temperatures.

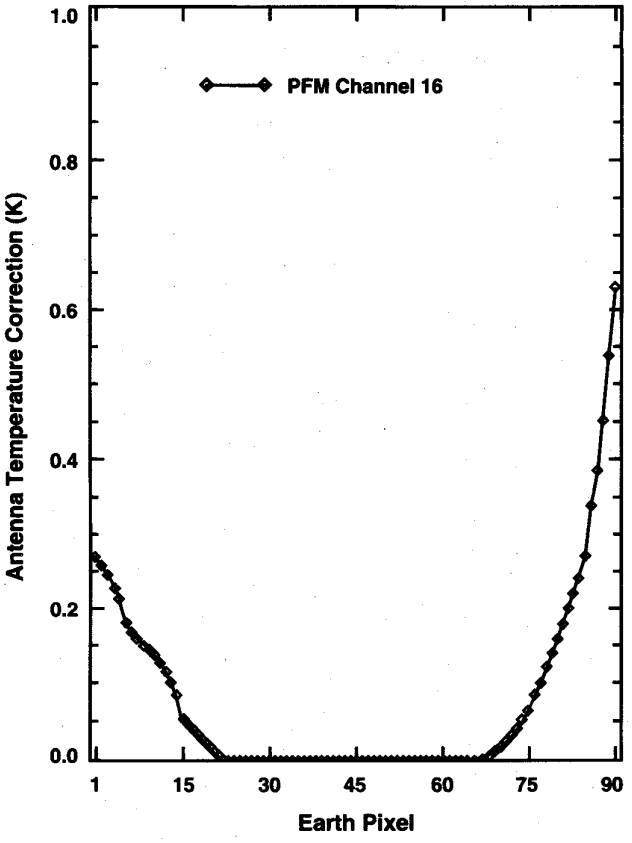

Fig. 7. Predicted antenna temperature corrections for a mean Earth scene brightness temperature of 230 K for channel 16 of the AMSU-B PFM. The correction should be added to the measured brightness temperatures.

16, 17, and 19 of the PFM assuming a mean Earth radiance equivalent to 230, 270, and 255 K, respectively (derived by averaging corresponding measured SSM/T-2 brightness temperatures of the Earth), and the platform with 100% reflectance at these frequencies. For channel 16, space view 3 clearly has the lowest radiance with least influence from the Earth and platform and is predicted to measure the equivalent of 3.6 K which is 0.9 K greater than the nominal microwave brightness temperature of space (2.73 K). For channels 17 and 19 space views 2 or 3 are predicted to be 0.4 and 0.7 K warmer than cold space. This difference between the predicted radiance and the space radiance for each channel gives a correction factor which must be included in the calculation of the space view radiance for the radiometric calibration to avoid a consistent bias in the radiometric gain. Once the instrument is in orbit the relative radiances in the four space views can be examined to verify these predictions and also to provide a better estimate of the mean Earth brightness temperature. The stability of the space radiance around an orbit and for different seasons will also need to be monitored to determine if this correction factor can be assumed to be a constant.

2) Effect on Earth Views: Similarly the Earth view radiances can be corrected for the effect of cold space and platform radiation in the antenna side lobes. This may become significant especially for fields of view on the edges of the swath where cold space radiance will reduce the measured Earth view radiances. The predictions for an assumed Earth brightness temperature of 230 K using the measured antenna pattern are shown as the points in Fig. 7 for channel 16 of the PFM. Pixels 1–25 are affected both by cold space and the warmer platform as shown in Fig. 5 and so the correction is reduced depending on the Earth radiance. On the space view side of the swath (pixels 70–90) only the cold space radiance influences these pixels and so the correction is larger than on the other side of the swath. The largest biases are for pixel 90 where for channel 16 the predicted reduction in the measured brightness temperature due to cold space in the side lobes is 0.6 K for a mean Earth radiance equivalent to 230 K. The effect will be larger for warmer Earth brightness temperatures.

VIII. Conclusion

The antenna patterns of the AMSU-B flight models have been measured on a Compact Antenna Test Range and all flight models met or were close to the required specifications. The main exceptions were channel 16 beam efficiencies being slightly less than required and channel 17 exceeding the 2% cross-polarization specification at one extreme of the scan. However, the extensive knowledge of AMSU-B's antenna performance based on the measurements reported here will allow accurate corrections to be applied to the data. Users

of AMSU-B data should find these measurements helpful to interpret the measured Earth radiances.

Based on predictions, using the measured antenna patterns, space view 3 is initially recommended for operational calibration, because it is predicted to suffer least from sidelobe contamination. The worst case increase in radiance for space view 3 is predicted to be equivalent to 0.9 K for channel 16 of PFM. The largest effect for the Earth views is a reduction in the measured radiance equivalent to 0.6 K for an Earth radiance equivalent to 230 K in pixel 90 at the edge of the swath. Closer to nadir these effects become negligible.

To refine the calculations of the effect of the spacecraft on the radiances, a better thermal model of the spacecraft is required in the vicinity of AMSU-B to better define the radiation seen in the sidelobes. Also, a near field antenna pattern analysis should be carried out to give a better estimate of the coupling between the parts of the spacecraft and the antenna. Both of these refinements are being implemented to improve the estimates of the corrections on the space view and Earth view radiances.

ACKNOWLEDGMENT

The authors would like to gratefully acknowledge the help of W. Simpson and the other MMS and QMW staff involved in the AMSU-B antenna tests.

REFERENCES

[1] R. W. Saunders, T. J. Hewison, S. J. Stringer, and N. C. Atkinson, "The radiometric characterisation of AMSU-B," *IEEE Trans. Microwave Theory Tech.*, vol. 43, pp. 760–771, Apr. 1995.

[2] T. Mo, J. Alishouse, N. Grody, and P. Taylor, "Antenna pattern data of AMSU-A protoflight model and flight model one," NOAA, Washington, DC, Tech. Memo. NOAA/NESDIS E/RA1, p. 17. (Available from T. Mo, NOAA, Washington, DC 20233).

[3] R. J. Martin and W. J. Hall, "Three dimensional design of quasioptical systems at BAe space systems," in *SPIE Int. Symp. Aerospace and Remote Sensing*, SPIE, Orlando, FL, 1993, vol. 1935, pp. 178–188.

[4] C. G. Parini and A. D. Olver, "Millimeter wave compact antenna test range," in *Proc. ISAP '92*, Sapporo, Japan, 1992, pp. 989–992.

[5] J. E. Charlton and M. L. Jarrett, "Antenna pattern measurements on AMSU-B," in *Proc. Microwave Instrumentation for Remote Sensing of the Earth*, SPIE, Orlando, FL, 1993, vol. 1935, pp. 199–208.

[6] M. Pilippakis and C. G. Parini, "Diffraction effects of a tape covering the gaps of a panelled compact range operating at millimeter wavelengths," in *IEE Proc. Microwaves and Antennas and Propagation*, 1994, vol. 141, pp. 114–122.

[7] F. T. Ulaby, R. K. Moore, and A. K. Fung, *Microwave Remote Sensing Active and Passive*, vol. I. Reading, MA: Addison-Wesley, 1981, pp. 94–106; pp. 203–205.

Timothy J. Hewison received the B.Sc. (Hons.) degree in physics with astrophysics from the University of Manchester, U.K., in 1989.

Since 1990, he has been with the Remote Sensing Instrumentation branch of the U.K. Meteorological Office. His work has included testing on the AMSU-B antennas, local oscillators, power spectra, and calibration targets and the development of a new microwave radiometer for the U.K. Meteorological Office C-130 research aircraft.

Roger Saunders received the Ph.D. degree in 1980 from Imperial College, University of London, U.K.

Since then he has worked in the field of satellite remote sensing at University College London, Rutherford Appleton Laboratories, U.K., and the European Space Operations Center, Darmstadt, Germany. He joined the U.K. Meteorological Office in 1984 and was the AMSU-B Project Scientist from 1992 to April 1995. He has recently moved to the European Centre for Medium Range Weather Forecasts, Reading, U.K., as Head of the satellite section.